Parametric Investigation on Simulated Staring FMCW Radar for Anti-Drone Swarms

Yun, Joongsup ; Anderson, David ; Fioranelli, Francesco

DOI
10.1109/RadarConf2043947.2020.9266354

Publication date
2020

Document Version
Accepted author manuscript

Published in
2020 IEEE Radar Conference, RadarConf 2020

Parametric Investigation on Simulated Staring FMCW Radar for Anti-Drone Swarms

Joongsup Yun
School of Engineering
University of Glasgow
Glasgow, UK
joongsup.yun@glasgow.ac.uk

David Anderson
School of Engineering
University of Glasgow
Glasgow, UK
dave.anderson@glasgow.ac.uk

Francesco Fioranelli
Department of Microelectronics
Delft University of Technology
Delft, The Netherlands
f.fioranelli@tudelft.nl

***Abstract*—This paper presents parametric investigation results on a staring FMCW radar system which targets drone swarms. The parametric investigation has been carried out by using the RAPID-SIM which facilitates system-level analysis of drone swarms' radar signatures. This paper explains concepts of the simulator's each module and also covers two parametric investigation results which deal with quantitative performance criteria for the design of the anti-drone swarms radar system.**

***Index Terms*—FMCW radar, staring radar, UAV, drone, swarms, Monte-Carlo simulation, rigid body kinematics**

I. Introduction

The use of small drones has increased explosively on both civilian and military sector in recent years. In terms of protecting life, property, and security of the nation from hostile drones, this situation has triggered growing demand for surveillance and defence systems targeting drones. Radar is frequently chosen as a main sensor for the surveillance system due to its robust performance in various lighting and weather conditions.

When the drone surveillance radar (DSR) system faces swarms of drones, its operational performance is limited by its operator's work intensity. The operator needs to identify each drone's intention and behaviour to determine if there is a potential to cause an emergency situation. In such a situation, we can consider introducing artificial intelligence (AI) as a way to alleviate or completely replace the operator's work.

The DSR can provides range-Doppler information which can be used to estimate presence, number, position, and velocity of drones. The estimation of intention and behaviour of drones can be made by such information on some level [1]. If we can classify drone's configuration and discriminate against a clutter like bird, performance of the estimation can be enhanced [2] [3]. Using micro-Doppler information is one of the possible solution of the drone classification because it reflects a rotor or a propeller configuration of each drone.

While previous researches have focused on the radar signatures of a single drone, the project RAPID (Radar Analysis and Prediction of Intentions/behaviour of small Drones' swarms) aims to develop a comprehensive simulator capable of modelling the radar signatures of multiple cooperating drones. The simulator currently under development for the project is referred to as RAPID-SIM (SIMulator of project RAPID) in this paper. The RAPID-SIM also capable of system-level analysis such as operational performance analysis or parametric sensitivity analysis. This can be done by using existing simulation engine MAVERIC (Modelling of Autonomous Vehicles using Robust Intelligent Computing) of University of Glasgow, which uses distributed artificial intelligence methods to simulate and perform various kinds of activities [4] [5].

Section II explains concepts of the RAPID-SIM's each module with key features and equations. Validation result of the RAPID-SIM is included in section III. Section IV shows two parametric analysis results: the first analysis deals with the design criterion for the classification algorithm aspect of a single drone and the second analysis deals with the design criterion for the tracking algorithm aspect of drone swarms condition.

This work has been supported by the US ONR-G (project RAPID).

978-1-7281-8942-0/20/$31.00 ©2020 IEEE

II. Simulation Framework

The RAPID-SIM consists of radar model, drone model, and parametric analysis tool.

A. Radar Model

Current version of the RAPID-SIM only have staring FMCW (Frequency-Modulated Continuous-Wave) model, however, other kinds of radar model can be implemented for future version. Detailed equation of the FMCW radar has been set based on [6]. Only key equations relating the parameter analysis on section IV is referred here. For the convenience of explanation, nominal radar has been defined as Table I. The radar is assumed to be a staring FMCW radar.

1) Antenna model: Total antenna gain G_a is given by

$$G_a = KG_d, \tag{1}$$

where K is directive gain and G_d is directivity gain. Assuming the beam has a circular cross section and has approximately 45% of power loss, the directivity gain is given by [7]

$$G_d = \frac{29,000}{\theta_1\theta_2}, \tag{2}$$

TABLE I
SPECIFICATIONS OF NOMINAL RADAR

Items	Value	Unit
Carrier frequency	8	GHz
Bandwidth	50	MHz
Pulse repetition frequency	3202	Hz
Sampling frequency	1069.5	kHz
Number of pulses for Doppler-FFT	60	N/A
Transmitter power	40	dBm

where θ_1 and θ_2 are beamwidth of horizontal and vertical, respectively. For a circular beam shape, θ_1 is equal to θ_2. For the nominal radar system, K has been set as follow equations.

$$K = \begin{cases} \cos(K\lambda_\psi) & \text{if } \cos(K\lambda_\psi) > 0.1 \\ 0.1 & \text{if } \cos(K\lambda_\psi) \leq 0.1 \end{cases} \tag{3}$$

Where λ_ψ is a horizontal line of sight angle of radar to target. The K is set to be 1.33 to have 90° HPBW(Half Power Bandwidth). That is,

$$K = \cos\left(1.33 \cdot \frac{\pi}{4}\right) \simeq 0.5. \tag{4}$$

2) Power Equation: Power of the received signal P_r is given by

$$P_r = \frac{P_t G_a^2 \lambda^2 \sigma}{(4\pi)^3 R^4}, \tag{5}$$

where P_t, λ, σ, R are transmitted power, wavelength of carrier, RCS(Radar Cross Section), and relative range, respectively. Power of thermal noise P_n is given by

$$P_n = kT_0FB_n, \tag{6}$$

where k, T_0, F, and B_n are Boltzmann's constant, standard temperature, noise figure, and noise bandwidth, respectively. Then, the SNR (Signal to Noise Ratio) of the radar is defined by

$$\text{SNR} = \frac{P_r}{P_n}. \tag{7}$$

B. Drone Model

The drone model consists of kinematics, guidance law, and RCS parts. It is assumed that several reflectors exist on both drone's fuselage and blades. Any configuration of UAVs, such as fixed-wing, helicopter, and multicopter in Fig. 1 can be implemented by changing kinematics models for blades' reflectors.

1) Kinematics: A drone's position $\mathbf{R}_d$, velocity $\mathbf{V}_d$, and attitudes can be computed seperately. The process to compute position and velocity of each reflectors are as follows.

On Fig. 2, R-frame is radar frame that is fixed on the ground. d-frame is drone's body-fixed frame. r_j-frame is j-th rotor-fixed frame which is rotating relative to d-frame. α is fuselage's reflector ID and β is blade's reflector ID.

For a reflector α, its position vector $\mathbf{R}_\alpha^R$ and velocity vector $\dot{\mathbf{R}}_\alpha^R$ on the R-frame are computed by

$$\mathbf{R}_\alpha^R = \mathbf{R}_d^R + \mathbf{C}_d^R \mathbf{r}_{d\alpha}^d \tag{8}$$

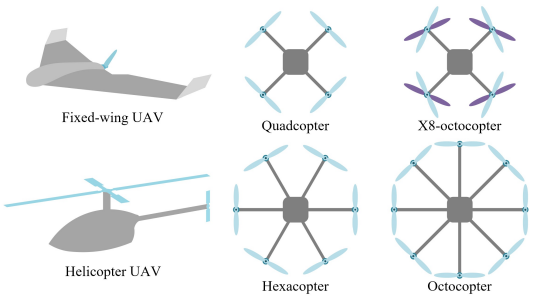

Fig. 1. Applicable configuration of UAVs

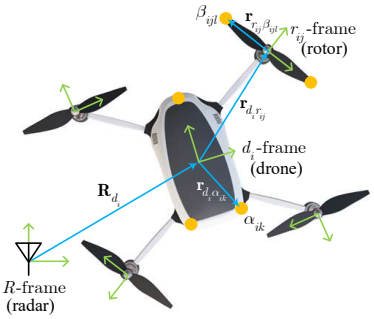

Fig. 2. Definitions of frames and position vectors

$$\dot{\mathbf{R}}_\alpha^R = \dot{\mathbf{R}}_d^R + \mathbf{C}_d^R \boldsymbol{\Omega}_{Rd}^d \mathbf{r}_{d\alpha}^d \tag{9}$$

where $\mathbf{C}_x^y$ is a direction cosine matrix which transfers vector on the x-frame to y-frame and $\boldsymbol{\Omega}_{xy}^y$ is defined as,

$$\boldsymbol{\Omega}_{xy}^y = [\boldsymbol{\omega}_{xy}^y]_\times = \begin{bmatrix} 0 & -\omega_3 & \omega_2 \\ \omega_3 & 0 & -\omega_1 \\ -\omega_2 & \omega_1 & 0 \end{bmatrix} \tag{10}$$

$$\boldsymbol{\omega}_{xy}^y = \begin{bmatrix} \omega_1 & \omega_2 & \omega_3 \end{bmatrix}^\intercal. \tag{11}$$

$\boldsymbol{\omega}_{xy}^y$ is an angular velocity vector of y-frame relative to x-frame, with respect to y-frame. Similarly, for a reflector β, its position vector $\mathbf{R}_\beta^R$ and velocity vector $\dot{\mathbf{R}}_\beta^R$ on the R-frame are computed by

$$\mathbf{R}_\beta^R = \mathbf{R}_d^R + \mathbf{C}_d^R \mathbf{r}_{dr}^d + \mathbf{C}_d^R \mathbf{C}_r^d \mathbf{r}_{r\beta}^r \tag{12}$$

$$\dot{\mathbf{R}}_\beta^R = \dot{\mathbf{R}}_d^R + \mathbf{C}_d^R \boldsymbol{\Omega}_{Rd}^d (\mathbf{r}_{dr}^d + \mathbf{C}_r^d \mathbf{r}_{r\beta}^r) + \mathbf{C}_d^R \mathbf{C}_r^d \boldsymbol{\Omega}_{dr}^r \mathbf{r}_{r\beta}^r \tag{13}$$

For updating of the cosine matrices, $\mathbf{C}_r^d$ and $\mathbf{C}_d^R$, we can use rotational vector algorithm introduced in [8].

2) Guidance Law: Any kind of guidance law can be implemented if it can provide trajectory of each drone's acceleration $\mathbf{A}_{d_i}(t)$. For example, if drone-1 has a straight trajectory and drone-2 has a constant speed(1 g) turn around the radar, the guidance laws of each drones can be defined as $\mathbf{A}_{d_1}(t) = 0$ and $\mathbf{A}_{d_2}(t) = -\frac{9.8}{|\mathbf{R}_{d_1}(t)|}\mathbf{R}_{d_1}(t)$. With given acceleration trajectory, each drones' position and velocity are computed by numerical integration algorithm such as Euler method or Runge-Kutta method.

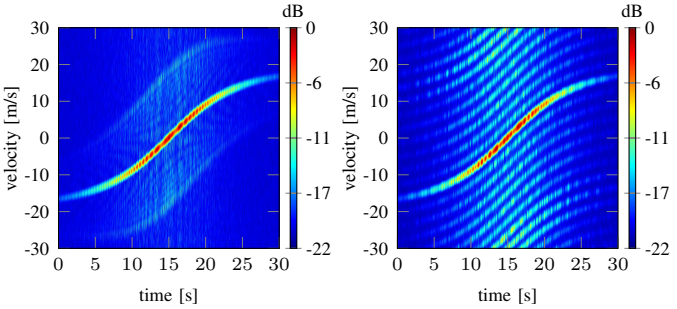

(a) fixed-wing UAV (b) quadcopter

Fig. 3. Micro-Doppler spectrogram of single drone

3) RCS of reflectors: Current version of the RAPID-SIM only consider statistical spot RCS model of each reflector to achieve high computational efficiency [9]. This model lacks of detailed electro-magnetic interaction between parts of a drone, such as multipath, vibration effects, and self-occlusion of parts. Approaches to increase both precision and computational efficiency of the scattering model is currently being studied. Upon the statistical RCS model, the RCS σ of (5) is not a stationary value for a dynamic situation. The Swerling model is a simple stochastic RCS model using the chi-distribution [10]. The Swering model has been adopted for the RCS model of current version of the RAPID-SIM.

To see the simulation performance of a single drone, a simple scenario has been set as in Fig. 4: a drone is crossing the front side of the radar from left to right. Two kinds of UAV will be following the trajectory line separately. During the simulation, two micro-Doppler spectrogram of both fixed-wing UAV and quadcopter drone has been generated as Fig. 3a and 3b. We can clearly observe the difference between two micro-Doppler signatures. The micro-Doppler signature of the fixed-wing UAV has narrow spread of blade reflectors' signal around the body reflector because the rotational speed of the propeller is 20 Hz. The micro-Doppler signature of the quadcopter has wide and strong spread of blade reflectors' signal around the body reflector because the rotational speed of the rotor is 100 Hz and the number of total reflectors on the blade is 8.

To see the simulation performance of multiple drones, a scenario has been set as in Fig. 5. The drone 1 and 3 are fixed-wing UAVs and the drone 2 is a quadcopter. Fig. 6a shows range measurements of three drones. We can observe strong intensity of the range-time graph when the drone is close to the radar. Fig. 6b shows micro-Doppler signatures where all of the signals from all range bins were superposed.

C. Parametric Analysis Tool

The parametric analysis tool can perform various kind of parametric analysis like performance analysis or sensitivity analysis. Fig. 7 shows general flow of the parametric analysis. The Parameter sweep is performed with deterministic value of each parameter, while the random parameter setting is needed for Monte-Carlo simulation. On the next section, two kinds of parametric analysis has been carried out.

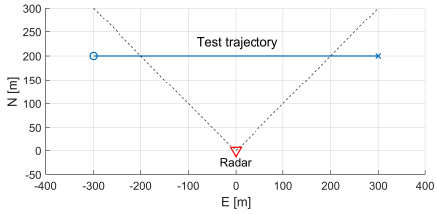

Fig. 4. Micro-Doppler test trajectory, where ○ marker is an initial position and × marker is final position.

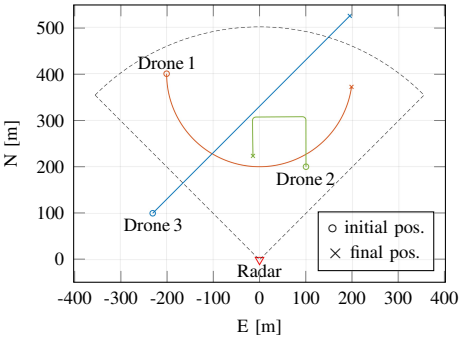

Fig. 5. Trajectories of three drones

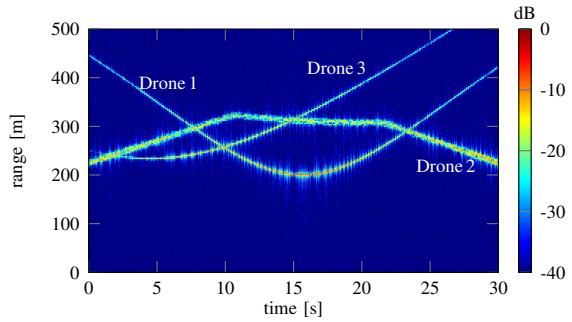

(a) range-time intensity

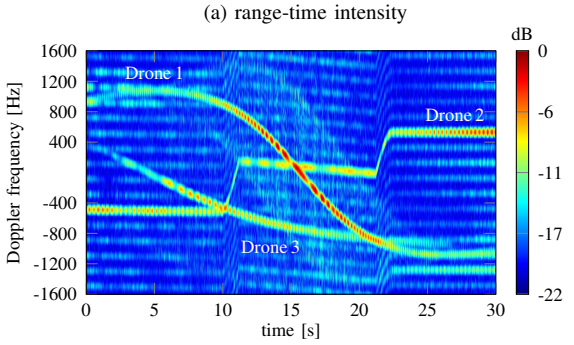

(b) micro-doppler spectrogram

Fig. 6. Radar measurement of three drones

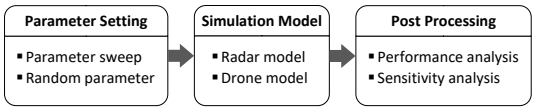

Fig. 7. Flow of parametric analysis

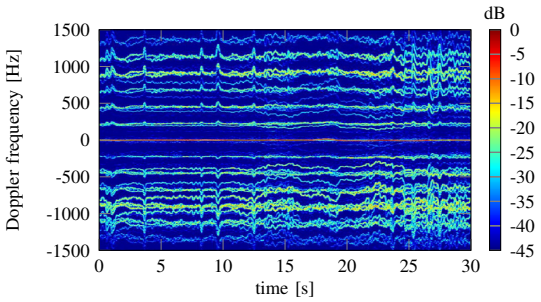

(a) NetRAD experimental data

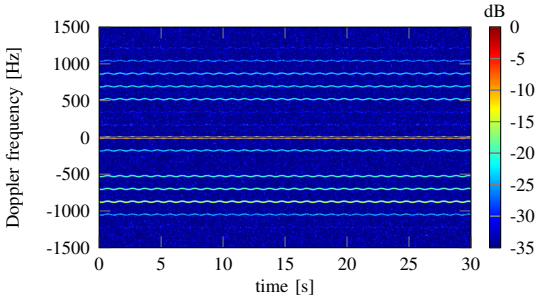

(b) RAPID-SIM

Fig. 8. Comparison of DJI Phantom's micro-Doppler spectrogram

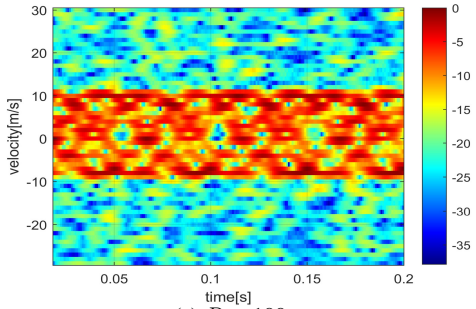

(a) $R = 100$m

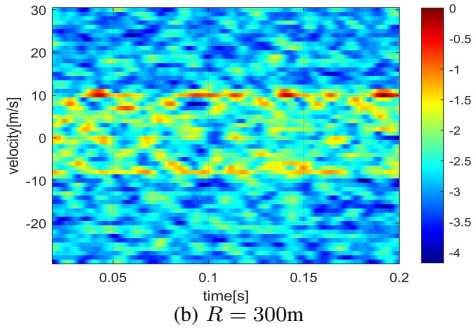

(b) $R = 300$m

Fig. 9. Micro-Doppler spectrogram of blade reflectors

III. Validation of Simulator

To validate the performance of the RAPID-SIM, an experimental result was used as reference data. The experiment was conducted using the multistatic pulsed radar system, NetRAD, developed by University College London and University of Cape Town [3]. The target was a DJI Phantom quadcopter hovering at approximately $70\,\mathrm{m}$ away from the radar. In the Fig. 8a, the experimental HERM(HElicopter Rotor Modulation) lines are fluctuating due to disturbances of the hovering control loop, such as irregular wind. Applying simplified fluctuation model using sinusoidal acceleration of the drone's centre of gravity, Fig. 8b shows similar HERM line distribution with respect to the Doppler gap between lines and the relative intensity of each lines.

IV. Parametric Analysis Result

A. Availability of Micro-Doppler

The micro-Doppler signature of a drone can be used to identify its class, configuration, or additional information, e.g weight of a payload [2]. However, micro-Doppler signature is not always available because it is made up by reflection of rotating parts which has relatively smaller RCS than fuselage's reflector has.

Using the developed simulation framework, micro-Doppler signal strength analysis of quadcopter's blade has been carried out. Fig. 9a and 9b are generated micro-Doppler spectrogram for $R = 100\,\mathrm{m}$, and $R = 300\,\mathrm{m}$ condition, respectively. Angular speed of the rotors are $10\,\mathrm{Hz}$ and each blade has two reflectors on their tips which have RCS of $-40\,\mathrm{dBsm}$. Radius of blade is $15\,\mathrm{cm}$. In this simulation, fuselage's reflector is not considered for the purpose of the analysis. We can clearly see that closer condition has higher SNR(signal to Noise Ratio) than farther condition has. If we could get high SNR signals, classification result will be more reliable. These phenomenon motivates a parametric analysis that provides design insight of a radar for target classification purpose. After changing of the angular speed of the rotors to more realistic value (about 100 Hz), Doppler-FFT result of the blade reflectors are depicted on Fig. 10 as a blue line. Thermal noise was not applied to generate the result. Inversely, orange line of Fig. 10 is a Doppler-FFT result of the thermal noise, without any reflector's signal. As Fig. 10 shows power spectral density function of the Doppler-FFT, we can directly compute band power of the blade reflector, BP_b and that of thermal noise, BP_t. Then, we can define the Doppler-FFT SNR(DSNR) as

$$\mathrm{DSNR} = \frac{\mathrm{BP}_b}{\mathrm{BP}_t}. \tag{14}$$

Fig. 11 shows the DSNR for various strength of transmitted power. If a minimum required DSNR condition is provided by classification algorithm, we can control the strength of transmitted power by the graph to meet the DSNR and maximum range condition simultaneously. For example, if currently designed P_t is $37\,\mathrm{dBm}$, minimum DSNR condition is $5\,\mathrm{dB}$, and the maximum classification range is $270\,\mathrm{m}$, we can see that we should increase the transmitted power by $6\,\mathrm{dB}$.

B. Maximum Trackable Number of Drones

Considering drone-swarms targets, the maximum trackable number of drone is important for the anti-drone purpose. One radar's maximum number of track is limited by its resolution of measurements. Then, for a range-Doppler radar, range resolution R_{res} and velocity resolution $V_{D,\mathrm{res}}$ are key parameters. Using these parameters, we can divide whole

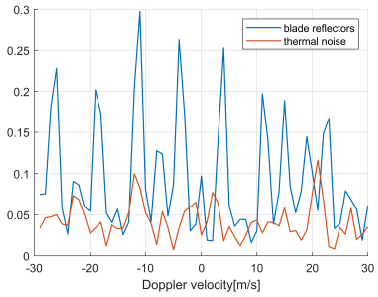

Fig. 10. Doppler-FFT signals of blade reflectors and thermal noise

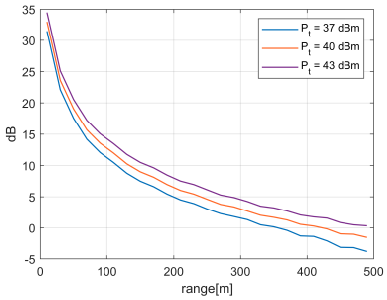

Fig. 11. Blade reflector's Doppler-FFT SNR for various transmitted power

range-Doppler map into multiple cells. To designate the single target's position on the range-Doppler map, CA-CFAR(Cell Average Constant False Alarm Rate) algorithm is usually used.

The data association is an algorithm that allocates updated CA-CFAR result to one of existing tracks [11]. Fundamental idea of data association is to make tracking gates for each target and use them as a track inclusion condition for updated measurement information. There has been developed various kind of gating algorithms on the academic field. However, common thing of all algorithm is that the tracking gates are computed based on the estimates of a target's motion and assumption of its manoeuvre model.

The estimates of range-Doppler radar are target's current relative range $R(t_1)$ and its rate of change, or radial velocity $V_r(t_1)$. For the purpose of simple gating, it is assumed that the target's manoeuvre model is the constant velocity one and we can estimate the speed of the target, $|\mathbf{V}|$, by using the Kalman filter. Let $\Delta\theta$ denotes heading uncertainty, which is caused by covariance of the filter and target's manoeuvre. Fig. 12 shows geometric definitions of the range and radial velocity gate. For the convenience of plotting, it is assumed that the updating period of radar estimates, Δt, is equal to 1 s. The range gate at t_2, $\mathbf{G}_R(t_2)$, is defined by

$$\mathbf{G}_R(t_2) \equiv [R_{\min}, R_{\max}], \tag{15}$$

where,

$$R_{\min} = \min\{|\mathbf{R}_{\text{nom}}|, |\mathbf{R}_+|, |\mathbf{R}_-|\} \tag{16}$$
$$R_{\max} = \max\{|\mathbf{R}_{\text{nom}}|, |\mathbf{R}_+|, |\mathbf{R}_-|\}, \tag{17}$$

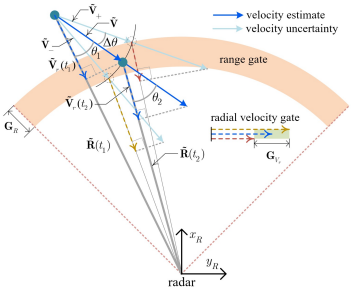

Fig. 12. Definition of range and radial velocity gate

and

$$\mathbf{R}_{\text{nom}} = \tilde{\mathbf{R}}(t_1) + \Delta t\tilde{\mathbf{V}} \tag{18}$$
$$\mathbf{R}_+ = \tilde{\mathbf{R}}(t_1) + \Delta t\tilde{\mathbf{V}}_+ \tag{19}$$
$$\mathbf{R}_- = \tilde{\mathbf{R}}(t_1) + \Delta t\tilde{\mathbf{V}}_-. \tag{20}$$

Denote that (16) and (17) are only valid for small $\Delta\theta$. The radial velocity gate at t_2, $\mathbf{G}_{V_r}(t_2)$, is defined by

$$\mathbf{G}_{V_r}(t_2) \equiv [V_{r,\min}, V_{r,\max}], \tag{21}$$

where,

$$V_{r,\min} = \min\{V_{r,\text{nom}}, V_{r,+}, V_{r,-}\} \tag{22}$$
$$V_{r,\max} = \max\{V_{r,\text{nom}}, V_{r,+}, V_{r,-}\}, \tag{23}$$

and

$$V_{r,\text{nom}} = (\mathbf{R}_{\text{nom}} \cdot \tilde{\mathbf{V}})/|\mathbf{R}_{\text{nom}}| \tag{24}$$
$$V_{r,+} = (\mathbf{R}_+ \cdot \tilde{\mathbf{V}})/|\mathbf{R}_+| \tag{25}$$
$$V_{r,-} = (\mathbf{R}_- \cdot \tilde{\mathbf{V}})/|\mathbf{R}_-|. \tag{26}$$

Using these definitions, tracking gate on the range-Doppler map is generated as in Fig. 13. On Fig. 13, red cells are single drone's current coordinates on the range-Doppler map and the green cells are gate areas defined by (15) and (21).

For multiple drones condition, let $\mathbf{G}_{R,d_i}$ and $\mathbf{G}_{V_r,d_i}$ denote range gate and radial velocity gate of a drone d_i, respectively. Using the gates of each drone, now we can define a probability that data association algorithm faces an ambiguity condition. Let $\mathbb{P}_{\text{RA}}$ denotes the probability of range ambiguity, which is defined by

$$\mathbb{P}_{\text{RA}} \equiv \mathbb{P}(\{R_{d_j}(t_2) \in \mathbf{G}_{R,d_i}(t_2) : i \neq j\}). \tag{27}$$

If there are n drones, $i \in [1, n]$ and $j \in [1, n]$. Similarly, let $\mathbb{P}_{\text{TA}}$ denotes the probability of radial velocity ambiguity, which is defined by

$$\mathbb{P}_{\text{VA}} \equiv \mathbb{P}(\{V_{r,d_j}(t_2) \in \mathbf{G}_{V_r,d_i}(t_2) : i \neq j\}). \tag{28}$$

We can consider that events of range ambiguity and radial velocity ambiguity are independent. Then, we can also define probability of tracking ambiguity $\mathbb{P}_{\text{TA}}$, which is defined by

$$\mathbb{P}_{\text{TA}} \equiv \mathbb{P}_{\text{RA}}\mathbb{P}_{\text{VA}}. \tag{29}$$

$\mathbb{P}_{\text{TA}}$ is a probability that the data association algorithm cannot simply allocate all of the updated measurements to

existing tracks because more than one measurements are within an identical gate. This is one of the main challenge for the data association algorithms to overcome, however, the $\mathbb{P}_{\mathrm{TA}}$ gives helpful information to a radar designer because the $\mathbb{P}_{\mathrm{TA}}$ can represent a worst performance of the data association algorithm. That is, to calculate the maximum trackable number of drones, one can use $\mathbb{P}_{\mathrm{TA}}$ for a quantitative criterion to calculate the value with an assumption of simplified tracking performance. Let $n_{\max}$ denotes the maximum trackable number of drones and T_P denotes the maximum value of allowable $\mathbb{P}_{\mathrm{TA}}$. Then, $n_{\max}$ can be defined by

$$n_{\max} \equiv \max\{n : \mathbb{P}_{\mathrm{TA}} \leq T_P\}. \tag{30}$$

Monte-Carlo simulations were carried out to see the effects of radar specifications on the maximum trackable number of drones. The number, initial positions, and initial velocities of drones of each Monte-Carlo runs were generated randomly. This means that all drones were assumed to have independent purpose from each other. Specific conditions for a drone cluster which has the same flight purpose can be modelled and applied in future work. Fig. 14 shows $\mathbb{P}_{\mathrm{TA}}$ with three cases of different bandwidths. We can confirm that the bandwidth B has a major effect on the maximum trackable number of drones, because the bandwidth affects the precision of the range cells. The larger the size of a single range cell, the higher the chance of the ambiguity condition. Assuming the T_P is 0.1, $n_{\max}$ is decreasing from 22 to 9 while the bandwidth is decreasing from $50\,\mathrm{MHz}$ to $10\,\mathrm{MHz}$.

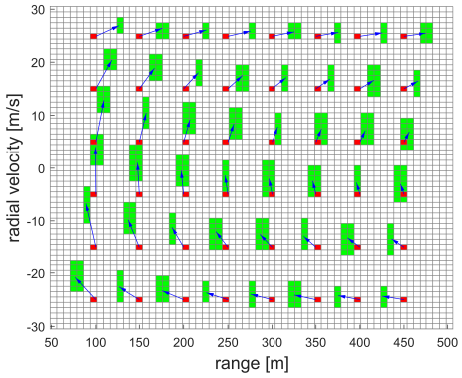

Fig. 13. Tracking gate on range-Doppler map, $B = 20\,\mathrm{MHz}$, $|\mathbf{V}| = 30\,\mathrm{m/s}$, $\Delta\theta = 5^\circ$

V. CONCLUSIONS

This paper has introduced a simulation framework for drone surveillance radar system, RAPID-SIM. The RAPID-SIM can simulate the radar signatures of drone swarms including micro-Doppler signatures. The research results of this project are expected to be useful in the development of target classification algorithms under the conditions of multiple drones. This paper also showed two parametric investigation results using The RAPID-SIM. The results of the analysis indicates that the RAPID-SIM can be used as a system-level design

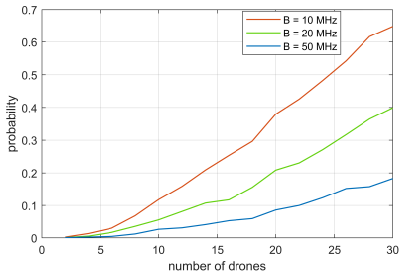

Fig. 14. $\mathbb{P}_{\mathrm{TA}}$ for three bandwidth

tool for design of anti-drone swarms radar. A limitation of the current version of the RAPID-SIM is the assumption of simplified RCS model. This will be overcome by application of various kinds of RCS model, such as thin-wire model [12] [13]. Reliability of the RAPID-SIM will also be improved by validation of it with experimental data for the future work. Furthermore, special attention will be given in modelling the kinematic of realistic swarm behaviours with the intricacies of mutual interactions and effects between different drones.

ACKNOWLEDGMENT

The authors acknowledge the support of the US ONR-G (project RAPID) for their work at the University of Glasgow on radar modelling and swarms of drones simulation.

REFERENCES

[1] F. Katsilieris and A. Charlish, "Knowledge based anomaly detection for ground moving targets," in *Proc. 2018 IEEE Radar Conference (RadarConf18)*, Oklahoma City, OK, USA, Apr. 2018, pp. 786–791.

[2] J. Patel, F. Fioranelli, and D. Anderson, "Review of radar classification and rcs characterisation techniques for small uavs or drones," *IET Radar, Sonar & Navigation*, vol. 12, pp. 911–919, Aug. 2018.

[3] J. Patel, C. Al-Ameri, F. Fioranelli, and D. Anderson, "Multi-time frequency analysis and classification of a micro-drone carrying payloads using multistatic radar," *IET The Journal of Engineering*, pp. 7047–7051, 2019.

[4] D. Anderson and K. Carson, "Integrated variable-fidelity modeling for remote sensing system design," *Technologies for Optical Countermeasures VI*, vol. 7483, pp. 615–622, Sep. 2009.

[5] M. Ireland and D. Anderson, "An investigation of the effects of model resolution on control of a quadrotor micro air vehicle," *International Journal of Unmanned Systems Engineering*, vol. 3, pp. 17–25, Jan. 2015.

[6] D. Barick, "FM/CW radar signals and digital processing," National Oceanic and Atmospheric Administration, Boulder Colorado, Tech. Rep. ERL 283-WPL 26, Jul. 1973.

[7] J. Hill, "Gain of directional antennas," *The Communications Edge*, p. 2, 2001.

[8] P. Groves, *Principles of GNSS, inertial, and multisensor integrated navigation systems*. London UK: Artech House, 2013, p. 42.

[9] R. Guay, G. Drolet, and J. Bray, "Rcs modelling of a mini-UAV based on dynamic measurements," in *Proc. 2017 IEEE Radar Conference (RadarConf17)*, Seattle, WA, USA, May 2017, pp. 786–791.

[10] P. Swerling, "Probability of detection for fluctuating targets," The RAND Corporation, Santa Monica California, Tech. Rep. RM-1217, Mar. 1954.

[11] A. Baruzzi and M. Martorella, "Multi-sensor multi-target tracking based on range-doppler measurement," *International Journal of Microwave and Wireless Technologies*, vol. 8, pp. 615–622, May 2015.

[12] Y. Cai, O. Krasnov, and A. Yarovoy, "Simulation of radar micro-Doppler patterns for multi-propeller drones," in *Proc. 2019 International Radar Conference*, Toulon, France, Sep. 2019.

[13] ——, "Radar recognition of multi-propeller drones using micro-Doppler linear spectra," in *Proc. 16th European Radar Conference*, Paris, France, Oct. 2019.